Disentangling the near-infrared continuum spectral components of the inner 500 pc of Mrk 573: two-dimensional maps

M. R. Diniz,[1][*] R. A. Riffel,[1] R. Riffel,[2] D. M. Crenshaw,[3] T. Storchi-Bergmann,[2] T. C. Fischer,[3,4] H. R. Schmitt[5] and S. B. Kraemer[6]

[1]*Universidade Federal de Santa Maria, Departamento de Física, Centro de Ciências Naturais e Exatas, 97105-900 Santa Maria, RS, Brazil*
[2]*Universidade Federal do Rio Grande do Sul, Instituto de Física, CP 15051, Porto Alegre 91501-970, RS, Brazil*
[3]*Department of Physics and Astronomy, Georgia State University, Astronomy Offices, 25 Park Place, Suite 605, Atlanta, GA 30303, USA*
[4]*Astrophysics Science Division, Goddard Space Flight Center, Code 665, Greenbelt, MD 20771, USA*
[5]*Naval Research Laboratory, Washington, DC 20375, USA*
[6]*Institute for Astrophysics and Computational Sciences, Department of Physics, The Catholic University of America, Washington, DC 20064, USA*

ABSTRACT

We present a near-infrared (near-IR) study of the spectral components of the continuum in the inner $500 \times 500 \, pc^2$ of the nearby Seyfert galaxy Mrk 573 using adaptive optics near-IR integral field spectroscopy with the instrument near-infrared integral field spectrograph of the Gemini North Telescope at a spatial resolution of $\sim$50 pc. We performed spectral synthesis using the STARLIGHT code and constructed maps for the contributions of different age components of the stellar population: young (age $\leq$100 Myr), young–intermediate ($100 <$ age ≤ 700 Myr), intermediate–old (700 Myr $<$ age ≤ 2 Gyr) and old (age > 2 Gyr) to the near-IR K-band continuum, as well as their contribution to the total stellar mass. We found that the old stellar population is dominant within the inner 250 pc, while the intermediate-age components dominate the continuum at larger distances. A young stellar component contributes up to $\sim$20 per cent within the inner $\sim$70 pc, while hot dust emission and featureless continuum components are also necessary to fit the nuclear spectrum, contributing up to 20 per cent of the K-band flux there. The radial distribution of the different age components in the inner kiloparsec of Mrk 573 is similar to those obtained by our group for the Seyfert galaxies Mrk 1066, Mrk 1157 and NGC 1068 in previous works using a similar methodology. Young stellar populations ($\leq$100 Myr) are seen in the inner 200–300 pc for all galaxies contributing with $\geq$20 per cent of the K-band flux, while the near-IR continuum is dominated by the contribution of intermediate-age stars ($t = 100$ Myr–2 Gyr) at larger distances. Older stellar populations dominate in the inner 250 pc.

Key words: galaxies: individual: Mrk 573 – galaxies: Seyfert – infrared: galaxies.

1 INTRODUCTION

Stellar population (SP) synthesis using multiwavelength spectra has been used to constrain the star formation history (SFH) of host galaxies of active galactic nuclei (AGN), looking in particular for the presence of recent star formation close to the AGN, supporting the so-called AGN–starburst connection (Perry & Dyson 1985; Terlevich & Melnick 1985; Norman & Scoville 1988). Indeed, previous studies have shown that massive star-forming regions are commonly detected in the inner kiloparsec of active galaxies (Imanishi & Dudley 2000; Storchi-Bergmann et al. 2000; Imanishi 2002;

Rodríguez-Ardila & Viegas 2003; Riffel et al. 2007, 2009b; Dors et al. 2008). Both, nuclear activity and star formation can be fed by gas inflows towards the nucleus, providing a gas reservoir in the central region of the galaxy. Indeed, inflows of gas have been observed using optical and near-infrared (near-IR) integral field spectroscopy (IFS) of nearby galaxies (e.g. Fathi et al. 2006; Riffel et al. 2008a; Fischer et al. 2015). This feeding process is associated with the presence of nuclear bars or non-axis-symmetric features, spiral arms, or tidal interactions (Knapen, Shlosman & Peletier 2000; Maciejewski et al. 2002; Maciejewski 2004a,b).

The SFH of galaxies can be used as a constraint for their formation and evolution, being a fundamental ingredient of theoretical models. Many studies of galaxy evolution in the IR spectral range are strongly based on evolutionary population synthesis (EPS)

* E-mail: diniz.mr@gmail.com

models (Capozzi et al. 2016). The main parameters of the SPs, as their ages, SFHs and stellar masses are derived through the EPS models. However, these models are still being refined and of particular importance is the contribution of thermally pulsing asymptotic giant branch (TP-AGB) stars that play an important role in defining the shape of the spectra in the near-IR wavelengths (e.g. Maraston 2005; Marigo et al. 2008; Salaris et al. 2014; Riffel et al. 2015). Constructing EPS models for evolved stars, such as TP-AGB stars, is not an easy task due to their complex inner structures, convection and the eventual mass ejections.

Recently, SP studies of nearby Seyfert galaxies using near-IR spectroscopy have become more frequent (e.g. Riffel et al. 2009b, and references therein). The near-IR spectral range, besides allowing us to access regions highly obscured by dust, also hosts spectral fingerprints originated in massive and evolved stars, as those found in the red supergiant and TP-AGB phases. These phases are responsible for a large fraction of the near-IR stellar continuum and can be used as tracers of young to intermediate SPs with ages between 200 Myr and 2 Gyr (Maraston 2005; Riffel et al. 2007, 2008b, 2015; Salaris et al. 2014). Additionally, in this spectral range, one can detect hot dust emission associated with the putative torus surrounding the central AGN, and some contribution also from the AGN featureless continuum (FC) emission, originated in the accretion disc (Riffel, Storchi-Bergmann & McGregor 2009c). The detection and characterization of these components is fundamental to understand the AGN spectral energy distribution and investigate the impact of the AGN in the evolution of its host galaxy.

For the reasons pointed out above, near-IR spectroscopy is a powerful tool to investigate both the SPs and the unresolved emission from the dusty torus and accretion disc surrounding the supermassive black hole (SMBH). With the aid of the integral field capability at 8–10 m telescopes, it is also possible to map the spatial distribution of the SP in the circumnuclear region of nearby active galaxies, a study that our group – AGNIFS (AGN integral field spectroscopy) – has been doing using the instrument NIFS (near-infrared integral field spectrograph) at the Gemini North Telescope.

In a recent work, we have used near-IR IFS and optical long-slit spectra to map the emission line and stellar kinematics of the inner 700×2100 pc^2 of Mrk 573 using the NIFS at Gemini North and Dual Imaging Spectrograph at Apache Point Observatory, respectively (Fischer et al. 2017). From this work, we found that flux distributions of ionized and molecular gas, while distinctly different, were morphologically related as arcs of molecular H$_2$ gas connected ionized [S III] gas features from outside the Narrow Line Region (NLR) bicone. We also found that molecular gas kinematics outside the NLR, and ionized gas kinematics at great distances from the nucleus in the extended NLR (ENLR), show signatures of rotation as observed from our stellar kinematics analysis. These observations suggest that the ionized gas kinematics and morphology in Mrk 573 can largely be attributed to material originating in the rotating disc of the host galaxy. Deviations from pure rotation were observed along the NLR projected axis at radii $r < 750$ pc and interpreted as being due to the radiative acceleration of material in the host disc. As the radiatively accelerated gas in the host disc goes to distances smaller than the length of the full NLR/ENLR, we concluded that these outflows may have a smaller range of impact than previously expected. The host disc galaxy presents an inclination of $i = 43°$, with the north edge corresponding to the side nearest to us (Fischer et al. 2017).

The stellar content of the central region of Mrk 573 was studied by Raimann et al. (2003) using long-slit spectra obtained with the 4-m Mayall telescope of Kitt Peak National Observatory. They oriented

the 1.5 arcsec width slit along the PA = 161° and mapped the SPs in the inner 8 arcsec (2.7 kpc). They found that the flux at 4020 Å is dominated by an old SP component. Within the inner 2 arcsec up to 70 per cent of the flux is due to emission of 10 Gyr SPs, while the contribution of these populations decreases at larger distances, being responsible for about 40 per cent of the observed flux at 8 arcsec from the nucleus. Intermediate-age (1 Gyr) SPs contribute with about 20 per cent of the nuclear flux, and their contribution increases to at larger distances, reaching 60 per cent outwards. The contribution of younger SPs is very small at all locations. The SP reddening values are in the range $E(B - V) = 0–0.4$, with the highest values seen at 2 arcsec south-east of the nucleus. On the other hand, Riffel et al. (2009b) found that the near-IR continuum in the inner 0.8 arcsec $\times$ 1.6 arcsec of Mrk 573 is dominated by intermediate-age populations with ages ranging from 100 Myr to 2 Gyr. The contribution of these populations reaches 53 per cent of the flux at 1.2 µm and is diluted by an FC component, which contributes with 22 per cent of the continuum. Ramos Almeida, Pérez García & Acosta-Pulido (2009) found also that intermediate-age stars dominate the near-IR nuclear continuum, but they did not found any evidence for the FC component.

This paper is organized as follows: in Section 2, we discuss the observations and data reduction procedures, Section 3 shows maps of the flux and mass-weighted contribution of each SP, which are discussed in Section 4. Section 5 summarizes the conclusions of this work.

2 OBSERVATIONS, DATA REDUCTION AND ANALYSIS

In this paper, we use the spectral synthesis technique to map the ages of the SPs of the inner 500 pc radius of the Seyfert 2 galaxy Mrk 573. Mrk 573 is a nearly face-on, early-type galaxy, morphologically classified as RSAB(rs)$^+$ (de Vaucouleurs et al. 1991), presenting a bright extended emission line region ($\sim$1 kpc) along the direction of its radio emission (Unger et al. 1987; Haniff, Wilson & Ward 1988) and high-ionization emission lines (Storchi-Bergmann et al. 1996). Three radio continuum sources were first detected by Ulvestad & Wilson (1984), one in the nucleus of the galaxy and the two radio lobes along position angle PA = 122°. It harbours a Seyfert 2 nucleus (Tsvetanov & Walsh 1992) and is located at a distance of $\sim$73 Mpc (Springob et al. 2005), for which 1 arcsec corresponds to 350 pc at the galaxy.

Z-, *J*- and *K*-band IFS of Mrk 573 have been obtained with the Gemini North NIFS (McGregor et al. 2003) operating with Gemini North Adaptive Optics system ALTAIR. Observations of Mrk 573 were obtained under the Gemini programme GN-2010B-Q-8 (PI: Michael Crenshaw) in 2010B and 2011A semesters, following the standard object-sky-object dither sequence. Six exposures of 600 s each were performed in the *K* band, centred at 2.3 µm and covering the spectral range from 2.1 to 2.5 µm, five exposures of 600 s for the *J* band, centred at 1.25 µm, covering the spectral region from 1.1 to 1.3 µm and six exposures of 500 s for the *Z* band, centred at 1.05 µm and covering the spectral region from 0.94 to 1.14 µm.

The NIFS has a square field of view of 3.0 arcsec $\times$ 3.0 arcsec, divided into 29 slices with an angular sampling of 0.10 arcsec $\times$ 0.04 arcsec, and was oriented along the position angle PA = 133°, measured relative to the orientation of the slices.

The data reduction was accomplished using tasks contained in the NIFS package, which are part of GEMINI IRAF package, as well as standard IRAF tasks and Interactive Data Language (IDL) routines. The process followed the standard procedure of near-IR spectroscopic

data reduction, including trimming of the images, flat-fielding, sky subtraction, wavelength and s-distortion calibrations. The telluric absorption bands were removed by dividing the spectra of the galaxy by a normalized spectrum of a telluric standard star, observed just before and/or after the galaxy exposures. The final spectra were then flux calibrated by interpolating a blackbody function to the spectrum of the telluric standard star. Individual exposure data cubes were created with an angular sampling of 0.05 arcsec × 0.05 arcsec, which were combined to obtain a single cube for each band, using the nucleus of the galaxy as reference for the astrometry. The final data cubes cover the inner ≈3.0 arcsec × 3.0 arcsec of Mrk 573, corresponding to ∼1 × 1 kpc² at the galaxy.

The spatial resolution is ∼45 pc for the *J* and *K* bands, as estimated from the full width at half-maximum (FWHM) of the brightness profile of the telluric standard star, while for the *Z* band the performance of ALTAIR is worse and the resulting spatial resolution is about 55 pc. The spectral resolution is ∼50 km s⁻¹ for all bands, as obtained from the typical FWHM of arc lamp lines.

Since the performance of the adaptive optics at the *Z* band is worse, compared with the *J* and *K* bands, and the signal-to-noise ratio of the *Z*-band continuum spectra is also lower, we used only the *J*- and *K*-band data cubes to perform the spectral synthesis. These cubes were combined to a single data cube with a constant spectral bin of 5 Å and 0.15 arcsec × 0.15 arcsec angular sampling. More details about the observations and data reduction procedure can be found in Fischer et al. (2017).

2.1 Spectral synthesis

The integrated spectrum of an active galaxy comprises a set of components such as stellar, gas, dust, as well as nuclear components such as a blackbody (from the torus) and power-law emission from the accretion disc. One way to disentangle these components is by the technique of spectral synthesis, which allows us to quantify the contributions of each one of these components to the spectrum.

A widely used code is the STARLIGHT (Cid Fernandes et al. 2004, 2005a,b; Asari et al. 2007), which fits the continuum searching for the best description of the observed spectrum by reproducing it with different proportions of the supposed components that sum up to the observed spectrum. These components comprise the base of spectral elements. In this way, the 'key' of the spectral synthesis technique is to provide a base of elements including all possible components observed in galaxies (Cid Fernandes et al. 2004, 2005a,b; Riffel et al. 2009a). When fitting near-IR spectral data one needs to have in mind that this region host characteristic absorption features, being the most common are the CN, CO, VO, ZrO and TiO absorption bands, which are attributed to evolved stars, as those in the RGB and TP-AGB phases (e.g. Maraston 2005; Riffel et al. 2007, 2015). Thus, the simple stellar population (SSP) models used to fit near-IR data need to include these features. Therefore, we selected the Maraston (2005) SSP models that include empirical data for the TP-AGB evolutionary phase.

The set of spectral elements used here is composed by the SSP models of Maraston (2005) and are described in Riffel et al. (2009b). In short, they include 12 ages (*t* = 0.01, 0.03, 0.05, 0.1, 0.2, 0.5, 0.7, 1, 2, 5, 9, 13 Gyr) and 4 metallicities (Z = 0.02, 0.5, 1, 2 Z_⊙). We also included blackbody functions for temperatures in the range 700–1400 K in steps of 100 K and a power law (F_λ ∼ λ⁻⁰·⁵), in order to account for possible contributions from hot dust emission and from an FC in the nucleus of the galaxy. For details, see Riffel et al. (2009a).

The fit is carried out in STARLIGHT by minimizing the following equation:

$$\chi^2 = \sum_\lambda [(O_\lambda - M_\lambda)\omega_\lambda]^2, \tag{1}$$

where O_λ is the observed spectrum, M_λ is the fitted model, $\omega_\lambda = 1/e_\lambda$ and e_λ corresponds to the associated uncertainties to the observed spectrum.

The emission lines and spurious data were excluded from the fit by setting their weight as zero. Each model spectrum is obtained by

$$M_\lambda = M_{\lambda 0} \left[\sum_{j=1}^{N_\star} x_j b_{j,\lambda} r_\lambda \right] \otimes G(\upsilon_\star, \sigma_\star), \tag{2}$$

where $M_{\lambda 0}$ is the synthetic flux at the normalization wavelength free of any emission or absorption line, x is the population vector, whose components x_j ($j = 1,\ldots, N_*$) represent the fractional contribution of each SSP in the spectral base, $b_{j,\lambda}$ is the normalized spectrum of the jth SSP component of the base, $\otimes$ corresponds the convolution operator and $G(\upsilon_\star, \sigma_\star)$ is the Gaussian distribution used to model the line-of-sight velocity distribution, centred at velocity $\upsilon_\star$ with dispersion $\sigma_\star$. The extinction due to dust is modelled as a uniform screen following the extinction law of Cardelli, Clayton & Mathis (1989).

3 RESULTS

An optical image of Mrk 573 obtained with the *Hubble Space Telescope* (*HST*) Wide Field Planetary Camera 2 through the filter *F*606*W* is shown in the top-left panel of Fig. 1. The central black square indicates the FOV of the NIFS observations. The right-hand panel shows a continuum image of the nuclear region, in logarithmic flux units per pixel, acquired from the NIFS data cube in the spectral range between 2.25 and 2.28 μm, without emission or absorption lines. Spectra from two positions (N and A), extracted within an aperture of 0.15 arcsec × 0.15 arcsec, are shown in the bottom panels. The central 'cross' corresponds to the location of the nucleus, which was defined as the peak of continuum emission.

The bottom panels of Fig. 1 show the results of the spectral synthesis overplotted to the observed spectrum (black), for the nucleus (N) and for position A, indicated on the continuum map (top-right panel). In the spectral synthesis, we masked out emission lines and spurious features, fitting only the regions with stellar absorption features and featureless continua.

The fits for all spaxels are very similar to those shown in Fig. 1. The quality of the fits can be evaluated using the rightmost panel of Fig. 3, where we show the map of the mean per cent deviation over all fitted pixels (Adev = |O_λ − M_λ|/O_λ).

Since small SP differences in the spectra are washed away due to the uncertainties on the observations, we have followed Cid Fernandes et al. (2004) and binned the contribution of the individual SSP, x_j, into a coarser population vector as follows (Riffel et al. 2009b, 2010): young (x_y: $t \leq 100$ Myr); young–intermediate (x_{yi}: $100 < t \leq 700$ Myr); intermediate–old (x_{io}: 700 Myr $< t \leq$ 2 Gyr) and old (x_o: $2 < t \leq 15$ Gyr).

Fig. 2 (top) shows the results of the spectral synthesis in maps of the main stellar population components (SPCs) per cent contributions to the 2.2 μm continuum light within inner ∼500 pc of Mrk 573. Grey regions in these maps correspond to masked locations where we were not able to get good fits, with Adev > 15. The x_y map shows that the young population contributes with up to
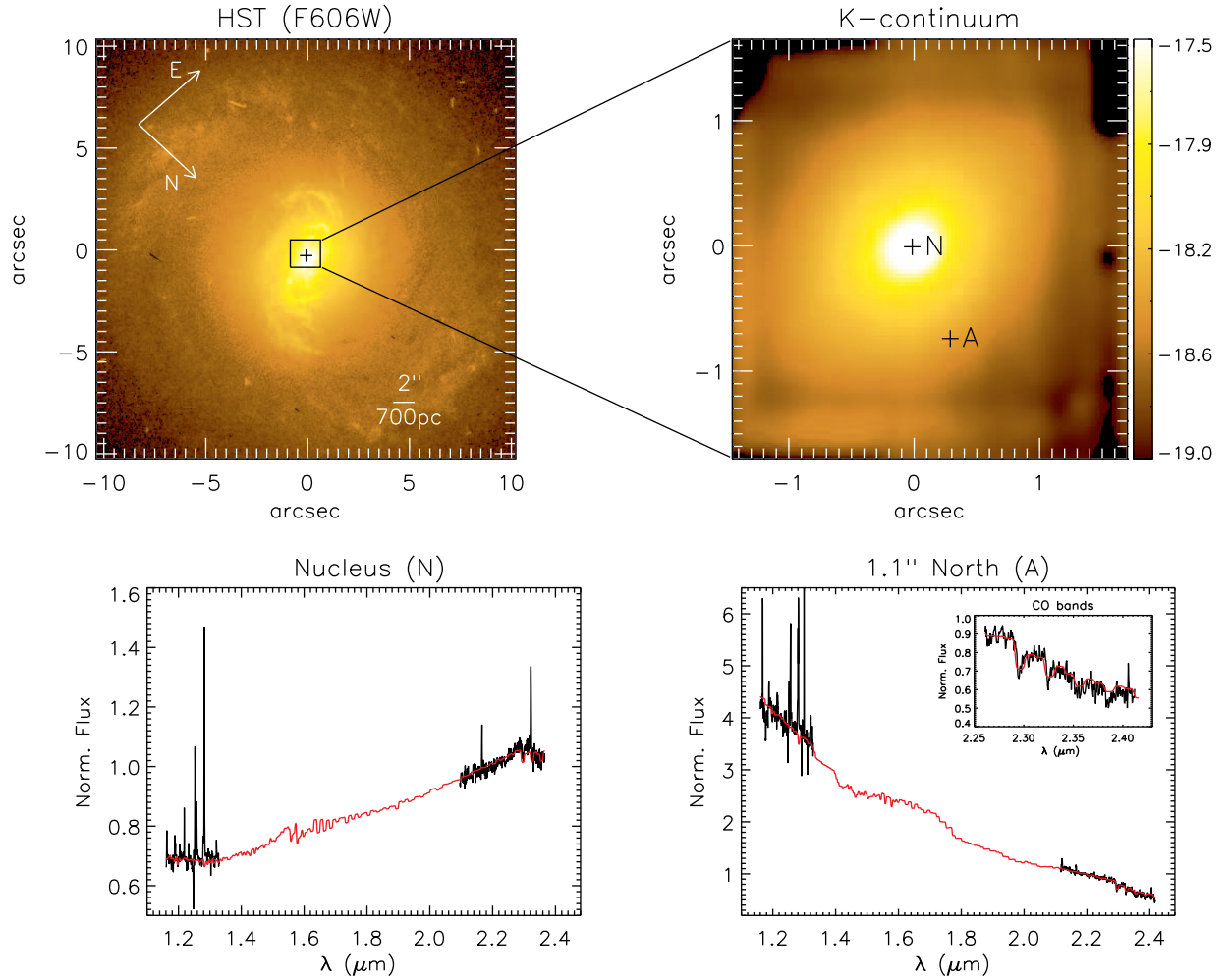
Figure 1. The left-hand panel shows an optical *HST* image of Mrk 573 through the filter *F606W*, with the NIFS FOV indicated by the central square. The right-hand panel displays a continuum image in the *K* band, in logarithmic flux units per pixel. The central cross on the panels indicates the position of the nucleus. The bottom panels show the synthesis results (red) for two spectra (black): the nucleus and position A identified in the top right panel. The flux was normalized at 21 955 Å and emission lines were masked. The *HST* image has been rotated to the same orientation of NIFS data (PA = 133°), indicated in the top-left corner of the top-left panel.

50 per cent of the continuum within ∼0.5 arcsec, with the highest contribution seen at 0.3 arcsec south of the nucleus. It decreases outwards and then increases again at ∼1 arcsec from the nucleus in a partial ring structure showing values of up to 100 per cent to the south and south-east. The rest of the ring is dominated by the contribution from the x_{yi} population that reaches up to 100 per cent at the ring. The last two panels (x_{io} and x_o) show a flux contribution of old SPs in the central region of up to 60 per cent mostly inside the ring.

Once the SSPs are in the form $L_\odot Å^{-1} M_\odot^{-1}$, thus a light-to-mass-ratio spectrum, the STARLIGHT code computes the mass fractions based on the L/M ratio.[1] The maps with the mass fractions for each binned age group are shown in the bottom panels of Fig. 2. The spatial distribution of each mass contribution, as expected, is similar to that observed to the light fractions; however, due to the non-linear M/L relation, the m_o maps show higher contributions in mass than in flux, with values of up to 95 per cent.

In Fig. 3, we present the maps for the FC and BB components that contribute to the observed continuum emission within 0.45 arcsec (180 pc). Although, by the map it seems that both have the same value, in fact the FC has a contribution of up to 35 per cent and the BB a contribution of up to 50 per cent, in the central pixels. In the same figure we show the $E(B - V)$ reddening map, which displays values of up to 0.8 and the Adev map with most of the values ≲10 per cent.

4 DISCUSSION

4.1 Distribution of the SPs

Studies of the SPs in nearby Seyfert galaxies based on near-IR long-slit spectra show a substantial fraction of intermediate-age SPs in the inner few hundreds of parsecs (e.g. Riffel et al. 2009b), while at optical wavelengths signatures of recent episodes of star formation are seen for about 40–50 per cent of nearby bright Seyfert 2 galaxies at similar spatial scales (e.g. Storchi-Bergmann et al. 2001; Raimann et al. 2003; Cid Fernandes et al. 2004; Sarzi et al. 2007). Young and intermediate-age SPs in the inner few hundreds of parsecs of Seyfert
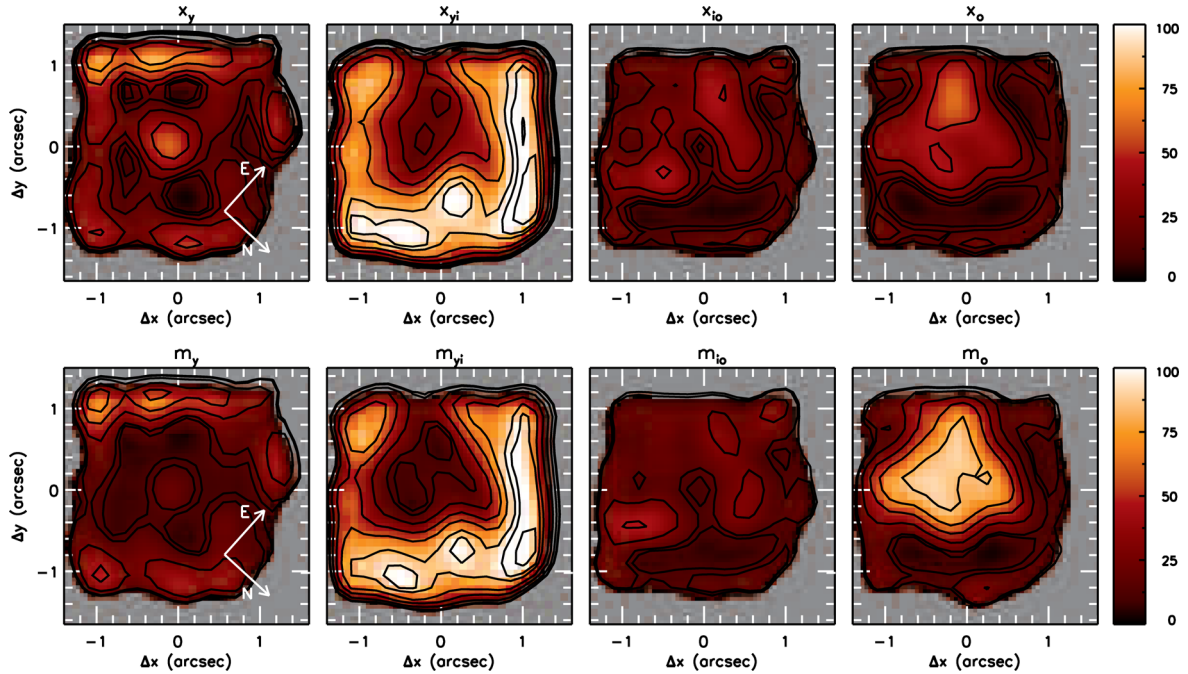
---

[1]More details can be found in the STARLIGHT user guide at http://www.starlight.ufsc.br.

Figure 2. From left to right, we show the distributions of: in the top row, per cent contributions to the 2.2 μm continuum of young ($x_y \leq 100$ Myr), young–intermediate ($100 < x_{yi} \leq 700$ Myr), intermediate–old (700 Myr $< x_{io} \leq 2$ Gyr) and old ($2 < x_o \leq 13$ Gyr) age components; In the bottom row, we show the corresponding per cent mass contributions (m_y, m_{yi}, m_{io} and m_o). The spatial orientation (PA = 133°) is indicated in the left-hand panels. Contours in the BB and FC panels correspond to 10 and 20 per cent flux contribution.

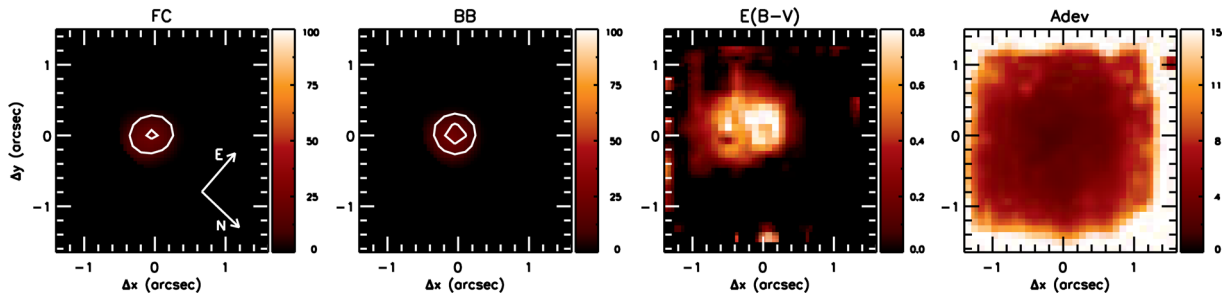**Figure 3.** From left to right: per cent contributions to the 2.2 μm continuum of the FC and BB emission, Adev and Av maps. The spatial orientation (PA =133°) is indicated in the left-hand panel.

galaxies are also detected in recent near-IR IFS studies (e.g. Davies et al. 2007; Riffel et al. 2010, 2011; Storchi-Bergmann et al. 2012). In addition, a correlation between the distribution of intermediate-age stars with low-stellar velocity dispersion ($\sigma_* \sim 50$–70 km s^{-1}) rings has been observed for some objects (Riffel et al. 2010, 2011), indicating that these low-σ_* rings are originated from SPs that still preserve the 'cold' kinematics of the gas they were formed (being thus younger than the surroundings), as claimed to explain the σ_*-drops commonly reported for more than 20 years (e.g. Emsellem et al. 2001; Márquez et al. 2003).

Our results for Mrk 573 show that old SPs are dominant in the inner 0.8 arcsec (300 pc), while at larger distances from the nucleus (up to $\approx$1.2 arcsec – covered by the FOV of our observations) young–intermediate SPs dominate the stellar mass and the K-band continuum emission (see Fig. 2). At optical wavelengths, Schmitt, Storchi-Bergmann & Cid Fernandes (1999) found that 82 per cent of the nuclear continuum at 5870 Å of Mrk 573 is due to a 10 Gyr SP. They used an integrated spectrum within an aperture of 2 arcsec × 2 arcsec and their result is in agreement with other studies of the SPs in optical wavelengths (Storchi-Bergmann et al. 2001; Raimann

et al. 2003). On the other hand, near-IR spectral synthesis of the nucleus for an aperture of 0.8 arcsec × 1.6 arcsec points out that intermediate-age stars contribute to 53 per cent of the K-band flux (Riffel et al. 2009a), being also in agreement with results obtained by Ramos Almeida et al. (2009), who found that the nuclear H- and K-band emission is dominated by late-type giants with ages between 100 Myr and 1 Gyr.

The simplest way to represent the mixture of SPs of a galaxy is estimating its mean light ($\langle \log t_* \rangle_L$) and mass ($\langle \log t_* \rangle_M$) weighted stellar age. Following Cid Fernandes et al. (2005a),

$$\langle \log t_\star \rangle_L = \sum_{J=1}^{N} x_j \log t_j \qquad (3)$$

and

$$\langle \log t_\star \rangle_M = \sum_{J=1}^{N} m_j \log t_j. \qquad (4)$$

While the former is more representative of younger ages, the latter is enhanced by the old SPC (Riffel et al. 2009b). In Fig. 4, we show the
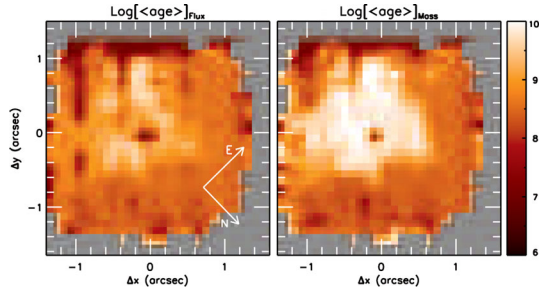
Figure 4. Logarithm of the mean age weighted by flux (left) and stellar mass (right).

maps for the mean age light- (left-hand panel) and mass-weighted (right-hand panel) in logarithmic units (years). The mean light- and mass-weighted ages over whole field of view are $\langle \log t_* \rangle_L = 8.39$ and $\langle \log t_* \rangle_M = 8.61$, respectively. These values are also in good agreement with those found in Riffel et al. (2009b) for the nuclear 0.8×1.6 arcsec.

As discussed above, studies based on seeing limited observations found that old SPs dominate the emission at optical bands, while in the near-IR intermediate-age stars are dominant (Schmitt et al. 1999; Storchi-Bergmann et al. 2001; Ramos Almeida et al. 2009; Riffel et al. 2009b). These studies are based on measurements of a nuclear spectrum that actually integrates the light within a few hundreds pc of the nucleus, which is comparable to the whole NIFS FOV. The NIFS adaptive optics observations allowed us to spatially resolve the distribution of the SPs in the inner 600 pc of Mrk 573 at a spatial resolution of ∼50 pc, at least five times better than that of the previous long-slit observations. We have shown that recent ($t < 700$ Myr) star formation dominates at distances larger than 300 pc from the nucleus (at least up to ≈500 pc from the nucleus), while at smaller distances older stars dominate the near-IR continuum emission and the stellar mass content of Mrk 573.

4.2 Spatial correlation among SPs, velocity dispersion and H_2 emission

Our group AGNIFS has started to characterize the SP of the inner kiloparsec of galaxies using the STARLIGHT code (e.g. Cid Fernandes et al. 2004, 2005a,b) via spectral synthesis of IFS obtained with the Gemini NIFS (McGregor et al. 2003). To date, we studied four nearby Seyfert galaxies (Mrk 1066, Mrk 1157, NGC 1068 and NGC 5548). For NGC 1068, we found two episodes of recent star formation: one at 300 Myr ago, extending over the inner 300 pc of the galaxy and another at 30 Myr ago, observed in a ring at ∼100 pc from the nucleus and being associated with an expanding ring observed in warm H_2 gas emission (Storchi-Bergmann et al. 2012). For Mrk 1066 and Mrk 1157, rings of intermediate-age stars have been found, being correlated with low stellar velocity dispersion values ($\sigma_* \sim 50$ km s^{-1}), and interpreted as being originated by stars that still preserve the kinematics of the gas from which they formed (Riffel et al. 2010, 2011). In the case of NGC 5548, the SP is dominated by an old (>2 Gyr) component between 160 and 300 pc from the nucleus, while closer to the nucleus, intermediate-age stars (50 Myr–2 Gyr) are dominant (Schönell et al. 2016). Hot dust emission was detected for three galaxies (Mrk 1066, NGC 1068 and NGC 5548), accounting for 30–90 per cent of the observed K-band nuclear flux, while for two galaxies the FC component was detected, contributing with ∼25 per cent of the K-band nuclear flux
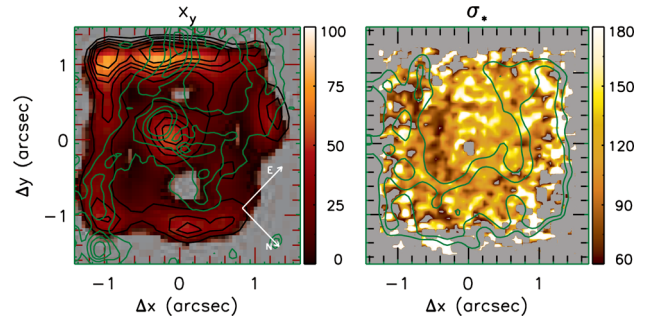

Figure 5. Map of the young SPC with green contours overlaid showing the $H_2 \lambda 2.12$ μm emission-line flux distribution (left-hand panel), and stellar velocity dispersion map (right-hand panel) with overlaid contours of the young–intermediate SPCs distributions in green.

for NGC 1068 and ∼60 per cent for NGC 5548 (Riffel et al. 2010, 2011; Storchi-Bergmann et al. 2012; Schönell et al. 2016).

In order to look for similar correlations for Mrk 573, we present in the left-hand panel of Fig. 5 contours (in green) of the $H_2 \lambda 2.1218$ μm flux distribution (left-hand panel) overlaid on the young SPC distribution, while in the right-hand panel we show the stellar velocity dispersion map with overlaid contours (in green) of the young–intermediate SPC. The $H_2 \lambda 2.1218$ μm fluxes were measured by direct integration of the H_2 line profile from the data cube and subtracting the adjacent continuum. The σ_* map was obtained by using the penalized pixel-fitting (pPXF) method of Cappellari & Emsellem (2004) to fit the CO absorption band-heads at ∼2.3 μm, using as templates spectra of late-type stars from Winge, Riffel & Storchi-Bergmann (2009). The H_2 flux distribution shows two arc-shaped structures extended along the east–west, with the highest emission observed within a blob centred at 0.3 arcsec south of the nucleus.

The σ_* map shows that most values range between 80 and 180 km s^{-1}, with the lowest values being observed mainly to south, west and north-west of the nucleus at distances of 0.5 arcsec from it. More details about the molecular gas distribution and kinematics and stellar kinematics are presented in Fischer et al. (2017).

Fig. 5 shows no clear correlation between the young SP distribution and the H_2 emission line map for Mrk 573, except maybe at 0.3 arcsec south of the nucleus where a blob of higher H_2 flux shows some overlap with the distribution of the young SPC around the nucleus. A similar trend is observed between low-σ_* values and the distribution of the young–intermediate-age SP, as shown by the green contours overplotted to the sigma map. This supports our previous similar findings for other active galaxies that the low-σ_* structures are due to stars formed ∼100–700 Myr ago, which are still not in orbital equilibrium with the bulge stars and were formed possibly from gas recently accreted to the inner kiloparsec (e.g. Barbosa et al. 2006).

4.3 Radial distribution of the SPs in Mrk 573 and comparison with other galaxies

In order to compare the radial distribution of SP contributions in Mrk 573 with those of previous studies by our AGNIFS team for other active galaxies, using similar data and technique, we have built radial profiles of the young, young–intermediate, intermediate–old and old population contributions to the flux at 2.2 μm for all studied galaxies so far. The results are shown in Fig. 6. The age bins for all galaxies are the same (as described in Section 3) and the derived
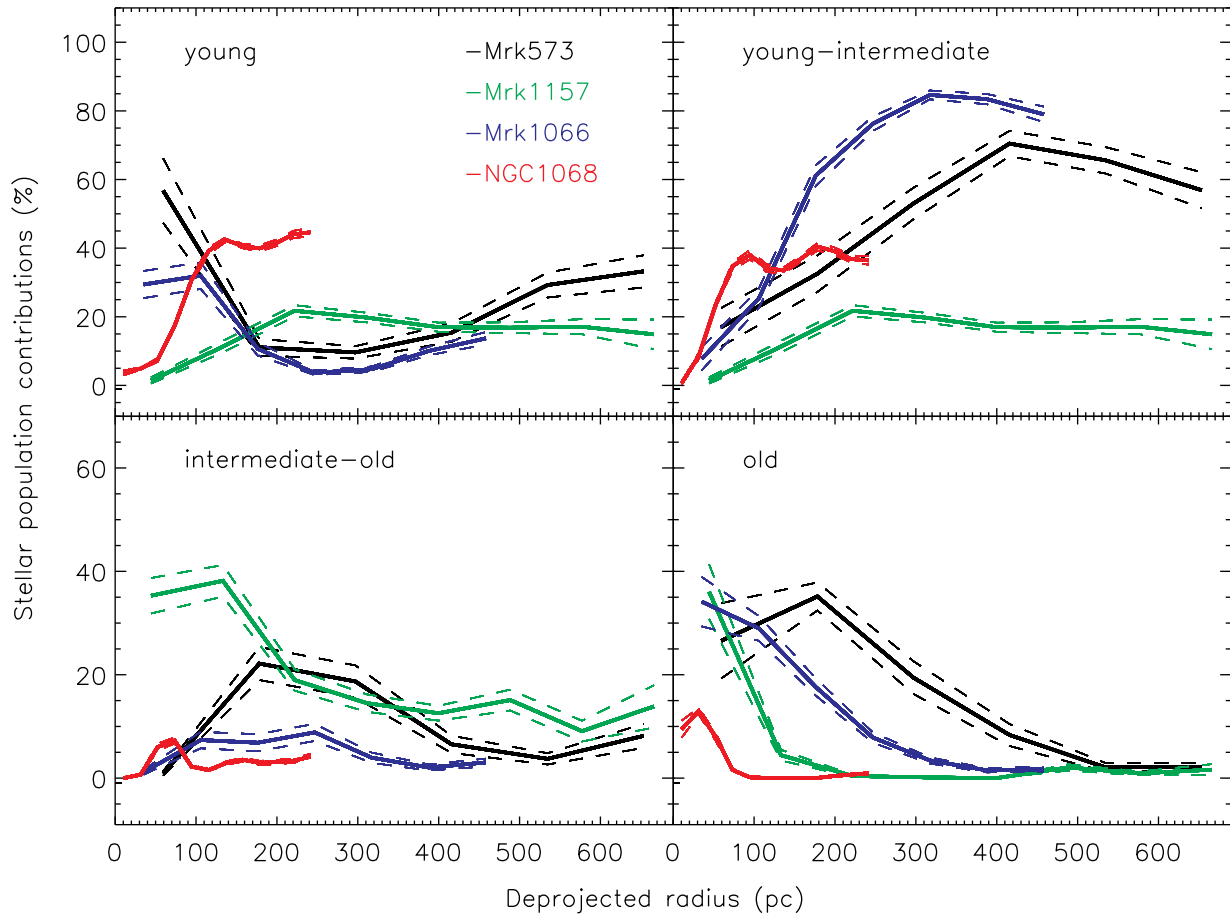
Figure 6. Contribution to the flux at 2.2 μm of each SP component as a function of the deprojected distance to the nucleus. Values for Mrk 573 are shown in black lines, for Mrk 1157 in green, for Mrk 1066 in blue and for NGC 1068 in red. The dashed lines show the standard deviation of the azimuthal mean at each radius. See text for more details.

values for Mrk 1066, Mrk 1157 and NGC 1068 are described in Riffel et al. (2010), Riffel et al. (2011) and Storchi-Bergmann et al. (2012), respectively. These plots were constructed by calculating the average contribution of each SPC to the flux at 2.2 μm within circular rings with 0.3 arcsec width in the (deprojected) plane of the disc of the galaxy. The orientation of the line of nodes (Ψ_0) and disc inclination (i) used in the deprojection were obtained from the modelling of the stellar velocity field and presented in Fischer et al. (2017) for Mrk 573 ($\Psi_0 = 97°$, $i = 26°$), Riffel et al. (2017) for Mrk 1066 ($\Psi_0 = 120°$, $i = 50°$) and Mrk 1157 ($\Psi_0 = 114°$, $i = 45°$) and Davies et al. (2007) for NGC 1068 ($\Psi_0 = 85°$, $i = 40°$).

Although contribution of young SPs of at least 20 per cent is observed at the nucleus only for Mrk 573 and Mrk 1066, they are present for all studied galaxies within the inner 200–300 pc, in good agreement with results obtained from optical (e.g. Storchi-Bergmann et al. 2001; Sarzi et al. 2007) and near-IR studies (e.g. Davies et al. 2007; Riffel et al. 2009a). These young stars possibly originate from a reservoir of gas recently accumulated in the central region of active galaxies. One possibility is that these reservoirs have been built by gas streaming motions along spiral arms and nuclear bars, seem at similar scales in many active galaxies (e.g. Fathi et al. 2006; Müller Sánchez et al. 2009; Diniz et al. 2015). The nuclear activity may also have been triggered by the presence of this gas reservoir, due to gas directly accreted by the SMBH or to accretion of gas ejected by the recently formed young stars (e.g. Davies et al. 2007; Riffel et al. 2009a).

Some contribution of young SPs is also observed at distances larger than 500 pc from the nucleus, while the young–intermediate-age SPs show their highest contribution at distances of 300–500 pc from it. The intermediate–old population is observed mainly within the inner 400 pc (with its highest contribution at ∼200–300 pc from the nucleus) and old populations are mainly observed within the inner 250 pc. The results for the oldest SPCs are in agreement with the inside out star formation scenario, in which a gradient of SP ages is observed, with old SPs seen at the nucleus and with decreasing ages outwards (Pérez et al. 2013; González Delgado et al. 2015, 2016).

4.4 Dust mass and AGN FC

We found that both the AGN FC (power-law) component and black-body emission contribute to up to 20 per cent of the observed *K*-band nuclear flux of Mrk 573, as seen in Fig. 3. The nucleus of Mrk 573 is classified as Seyfert 2 and the inclusion of these components is necessary to fit the nuclear spectrum of at least 25 per cent of Seyfert 2 galaxies, while more than 50 per cent of Seyfert 1 galaxies show FC and hot dust contribution (Riffel et al. 2009b). The detection of the power-law component for Mrk 573 suggests that radiation from the accretion disc is coming out through the torus, in good agreement with the detection of an obscured narrow-line Seyfert 1 nucleus as indicated by the presence of a broad component in the Pa β emission line (Ramos Almeida et al. 2008).

The spectral synthesis confirmed the presence of an unresolved blackbody component at the nucleus, previously detected in the IR (Ramos Almeida et al. 2009; Riffel et al. 2009b; Schlesinger et al. 2009), and possibly due to the dusty torus surrounding the SMBH. We have estimated the mass of the hot dust following Riffel et al. (2009a) and using the formalism of Barvainis (1987), for dust composed by grains of graphite.

The IR spectral luminosity of each dust grain, in erg s^{-1} Hz^{-1}, can be written as

$$L_{\nu,\mathrm{ir}}^{\mathrm{gr}} = 4\pi^2 a^2 Q_\nu B_\nu(T_{\mathrm{gr}}), \tag{5}$$

where $a = 0.05$ μm is the grain radius, $Q_\nu = 1.4 \times 10^{-24}\nu^{1.6}$ is its absorption efficiency and $B_\nu(T_{\mathrm{gr}})$ is its spectral distribution assumed to be a Planck function for a temperature T_{gr}.

The total number of graphite grains can be obtained from

$$N_{\mathrm{HD}} \sim \frac{L_{\mathrm{ir}}^{\mathrm{HD}}}{L_{\mathrm{ir}}^{\mathrm{gr}}}, \tag{6}$$

where $L_{\mathrm{ir}}^{\mathrm{HD}}$ is the total luminosity of the hot dust, obtained by integrating the flux of each blackbody component contribution from the synthesis. Then, we multiplied the integrated normalized flux by the normalization flux at 21 955 Å and convert it to the adequate units (from erg s^{-1} cm^{-2} Å^{-1} to erg s^{-1} Hz^{-1}). In order to obtain $L_{\mathrm{ir}}^{\mathrm{gr}}$, we have integrated equation (5) for all temperatures, ranging them from 700 to 1400 K, in steps of 100 K.

Finally, the hot dust mass can be obtained by the equation (e.g. Rodríguez-Ardila, Contini & Viegas 2005):

$$M_{\mathrm{HD}} \sim \frac{4\pi}{3} a^3 N_{\mathrm{HD}} \rho_{\mathrm{gr}}, \tag{7}$$

where $\rho_{\mathrm{gr}} = 2.26$ g cm^{-3} is the density of the grain. The total dust mass estimated for the nucleus of Mrk 573 by integrating over the entire field of view is $M_{\mathrm{HD}} = 1.3 \times 10^{-2}$ M$_\odot$, which is within the range of masses observed for other active galaxies (e.g. Rodríguez-Ardila et al. 2005; Rodrígues-Ardila & Mazzalay 2006; Riffel et al. 2009b, 2010, 2011).

4.5 Extinction

The $E(B - V)$ map (Fig. 3) obtained for the SP shows higher values to the south-west side of the nucleus. We can compare this map with that for the gas extinction. A gas reddening map can be obtained by using the Pa β/Br γ emission line ratio via the following equation:

$$E(B - V) = 4.74 \log\left(\frac{5.88}{F_{\mathrm{Pa}\beta}/F_{\mathrm{Br}\gamma}}\right), \tag{8}$$

where $F_{\mathrm{Pa}\beta}$ and $F_{\mathrm{Br}\gamma}$ are the fluxes of Pa β and Br γ emission lines, respectively. This equation was obtained using the reddening law of Cardelli et al. (1989) and adopting the intrinsic ratio $F_{\mathrm{Pa}\beta}/F_{\mathrm{Br}\gamma} = 5.88$ corresponding to case B recombination (Osterbrock & Ferland 2006). The Pa β and Br γ emission line flux distributions were obtained by fitting the line profiles at each spaxel by Gaussian curves, and as discussed in Fischer et al. (2017) these lines show similar flux distributions to those of the [S III]λ0.95 μm line. The resulting $E(B - V)$ map for the gas is shown in Fig. 7.

The median value of the reddening for the gas over the whole field of view is $E(B - V) \sim 2.5$ mag, considering only spaxels where both Br γ and Pa β emission lines were detected. For the SP, we obtain a smaller value of $E(B - V) \sim 0.25$ mag by averaging the map presented in Fig. 3, showing that the gas extinction in the NLR is larger than that of the SP. Riffel, Rodríguez-Ardila & Pastoriza (2006) presented the nuclear spectrum of Mrk 573 for an aperture of 0.8 arcsec × 1.6 arcsec obtained with the spectrograph SpeX covering the spectral range from 0.8 to 2.4 μm. Using their flux values for Br γ and Pa β emission lines, we obtain an $E(B - V)$ value for the gas very similar to ours, while Riffel et al. (2009b) obtained $E(B - V) \approx 0.3$ mag for the SP using the same data set. A higher extinction for the gas is also observed at optical wavelengths, in which the optical depth of the continuum underlying the Balmer lines is about half of that for the emission lines (Calzetti, Kinney & Storchi-Bergmann 1994). This difference may be due to the fact that most of the gas is located closer to the galaxy disc, where large amount of dust is expected, while the near-IR continuum has an important contribution from stars of the bulge of the galaxy.

Comparing the gas and stellar $E(B - V)$ maps, we note that they show a similar distribution near the nucleus, with higher values observed to the south-west of the nucleus and values close to zero to the north-east of it. The observed extinction for the gas is larger than that of the SP, in good agreement with previous studies (e.g. Riffel et al. 2008b). A higher extinction to the south-west of the nucleus is also supported by the dust lanes seen in the structure map presented in fig. 7 of Fischer et al. (2017).

The rightmost panel of Fig. 7 shows that the distribution of the hot molecular gas presents a good correlation with the gas $E(B - V)$, confirming the known association between the molecular gas and dust. The highest apparent concentration of hot molecular gas coincides with the region of highest extinction in the gas and in the stars at 0.3 arcsec south of the nucleus, being also co-spatial with young SPs (Fig. 2).
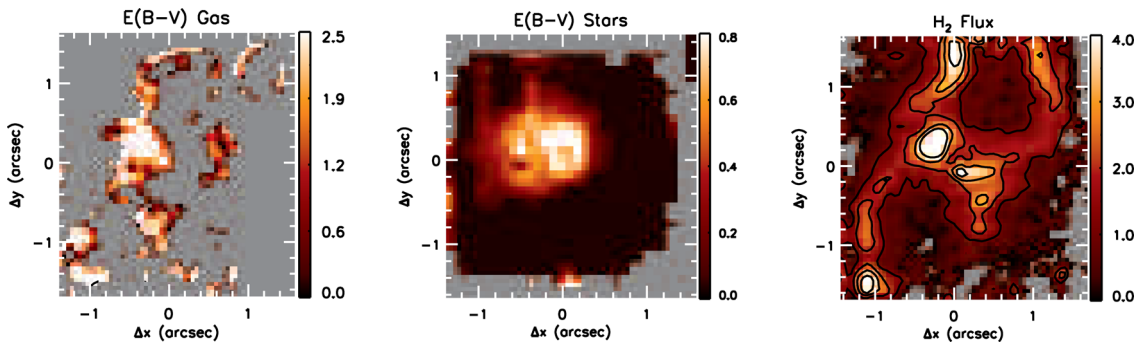

Figure 7. From left to right: $E(B - V)$ map for the gas from the line ratios between Pa β and Br γ; stellar $E(B - V)$ map obtained from STARLIGHT and the H$_2$ 21 218 Å flux map.

5 CONCLUSIONS

We used near-IR integral field spectra at a spatial resolution of ∼50 pc to map the SP distributions in the inner 500 pc of the Seyfert galaxy Mrk 573, as well as featureless continua contributions at the nucleus by combining the spectral synthesis technique with Maraston (2005) SSP models. The main conclusions of this work are as follows.

(i) Although the old SP ($x_i > 2$ Gyr) dominates the K-band continuum in the inner ∼250 pc (0.75 arcsec), within the ∼70 pc from the nucleus there is up to 30 per cent contribution from a young SP ($x_i < 100$ Myr). Beyond the inner ∼250 pc and up to the border of the FOV (500 pc), the young–intermediate-age SPs (100–700 Myr) are dominant, in a structure resembling a partial ring where its contribution to the continuum reaches up to ≈ 100 per cent in the K band.

(ii) Unresolved power-law and blackbody functions contributions to the continuum are detected at the nucleus at the level of 20 per cent in the K band. The first is attributed to the accretion disc emission and the latter to the emission from the dusty torus. We derive a hot dust mass of ∼0.013 $M_{\odot}$, consistent with values observed for other Seyfert 2 galaxies.

(iii) The distribution of intermediate-age stars shows a weak correlation with locations where we observe low stellar velocity dispersion values, supporting that these low-σ structures are originated in SPs that still preserve the cold kinematics of the gas from which they were formed.

(iv) By comparing the radial distribution of each SP component observed in Mrk 573 with those of other three galaxies studied using similar data (Mrk 1066, Mrk 1157 and NGC 1068), we found that young SPs (contributing with ≥ 20 per cent of the K-band continuum) are observed for all galaxies within the inner 200–300 pc, while intermediate-age stars dominate the near-IR K-band continuum at distances between 100 and 500 pc. Old SPs are dominant for distances smaller than 300 pc.

(v) The SP extinction is larger at the nucleus and to the southwest of it, where we also observe higher gas extinction, as derived from the Pa β/Br γ line ratio. The high extinction region to the south-west coincides also with a region of strong hot molecular gas emission.

REFERENCES

Asari N. V., Cid Fernandes R., Stasińska G., Torres-Papaqui J. P., Mateus A., Sodré L., Schoenell W., Gomes J. M., 2007, MNRAS, 381, 263
Barbosa F. K. B., Storchi-Bergmann T., Cid Fernandes R., Winge C., Schmitt H., 2006, MNRAS, 371, 170
Barvainis R., 1987, ApJ, 320, 537
Calzetti D., Kinney A. L., Storchi-Bergmann T., 1994, ApJ, 429, 582
Capozzi D., Maraston C., Daddi E., Renzini A., Strazzullo V., Gobat R., 2016, MNRAS, 456, 790
Cappellari M., Emsellem E., 2004, PASP, 116, 138
Cardelli J. A., Clayton G. C., Mathis J. S., 1989, ApJ, 345, 245
Cid Fernandes R., Gu Q., Melnick J., Terlevich E., Terlevich R., Kunth D., Rodrigues Lacerda R., Joguet B., 2004, MNRAS, 355, 273
Cid Fernandes R., González Delgado R. M., Storchi-Bergmann T., Martins L. P., Schmitt H., 2005a, MNRAS, 356, 270
Cid Fernandes R., Mateus A., Sodré L., Stasińska G., Gomes J. M., 2005b, MNRAS, 358, 363
Davies R. I., Sánchez F. M., Genzel R., Tacconi L. J., Hicks E. K. S., Friedrich S., Sternberg A., 2007, ApJ, 671, 1388
de Vaucouleurs G., de Vaucouleurs A., Corwin H. G., Jr, Buta R. J., Paturel G., Fouqué P., 1991, Third Reference Catalogue of Bright Galaxies RC3. Springer-Verlag, New York
Diniz M. R., Riffel R. A., Storchi-Bergmann T., Winge C., 2015, MNRAS, 453, 1727
Dors O. L., Storchi-Bergmann T., Riffel, Rogemar A., Schmidt A., 2008, A&A, 482, 59
Emsellem E., Greusard D., Combes F., Friedli D., Leon S., Pécontal E., Wozniak H., 2001, A&A, 368, 52
Fathi K., Storchi-Bergmann T., Riffel R. A., Winge C., Axon D. J., Robinson A., Capetti A., Marconi A., 2006, ApJ, 641, 25
Fischer T. C., Crenshaw D. M., Kraemer S. B., Schmitt H. R., Storchi-Bergmann T., Riffel R. A., 2015, ApJ, 799, 234
Fischer T. C. et al., 2017, ApJ, 834, 30
González Delgado R. M. et al., 2015, A&A, 581, 44
González Delgado R. M. et al., 2016, A&A, 590, 17
Haniff C. A., Wilson A. S., Ward M. J., 1988, ApJ, 334, 104
Imanishi M., 2002, ApJ, 569, 44
Imanishi M., Dudley C. C., 2000, ApJ, 545, 701
Knapen J. H., Shlosman I., Peletier R. F., 2000, ApJ, 529, 93
McGregor P. J. et al., 2003, in Iye M., Moorwood A. F. M., eds, Proc. SPIE Conf. Ser. Vol. 4841, Instrument Design and Performance for Optical/Infrared Ground-based Telescopes. SPIE, Bellingham, p. 1581
Maciejewski W., 2004a, MNRAS, 654, 883
Maciejewski W., 2004b, MNRAS, 654, 892
Maciejewski W., Teuben P. J., Sparke L. S., Stone J. M., 2002, MNRAS, 329, 502
Maraston C., 2005, MNRAS, 362, 799
Marigo P., Girardi L., Bressan A., Groenewegen M. A. T., Silva L., Granato G. L., 2008, A&A, 482, 883
Márquez I., Masegosa J., Durret F., González Delgado R. M., Moles M., Maza J., Pérez E., Roth M., 2003, A&A, 409, 459
Müller Sánchez F., Davies R. I., Genzel R., Tacconi L. J., Eisenhauer F., Hicks E. K. S., Friedrich S., Sternberg A., 2009, ApJ, 691, 749
Norman C., Scoville N., 1988, ApJ, 332, 124
Osterbrock D. E., Ferland G. J., 2006, Astrophysics of Gaseous Nebulae and Active Galactic Nuclei, 2nd edn. University Science Books, Mill Valley, CA
Pérez E. et al., 2013, ApJ, 764, 1
Perry J. J., Dyson J. E., 1985, MNRAS, 213, 665
Raimann D., Storchi-Bergmann T., González Delgado R. M., Cid Fernandes R., Heckman T., Leitherer C., Schmitt H. R., 2003, MNRAS, 339, 772
Ramos Almeida C., Pérez García A. M., Acosta-Pulido J. A., Gónzalez-Martín O., 2008, ApJ, 680, L17
Ramos Almeida C., Pérez García A. M., Acosta-Pulido J. A., 2009, ApJ, 694, 1379
Riffel R., Rodríguez-Ardila A., Pastoriza M. G., 2006, A&A, 457, 61

Riffel R., Pastoriza M. G., Rodríguez-Ardila A., Maraston C., 2007, ApJ, 659, 103

Riffel R. A., Storchi-Bergmann T., Winge C., McGregor P. J., Beck T., Schmitt H., 2008a, MNRAS, 385, 1129

Riffel R., Pastoriza M. G., Rodríguez-Ardila A., Maraston C., 2008b, MN-RAS, 388, 803

Riffel R. A., Storchi-Bergmann T., Dors O. L., Winge C., 2009a, MNRAS, 393, 783

Riffel R., Pastoriza M. G., Rodríguez-Ardila A., Bonatto C., 2009b, MN-RAS, 400, 273

Riffel R. A., Storchi-Bergmann T., McGregor P. J., 2009c, ApJ, 698, 1767

Riffel R. A., Storchi-Bergmann T., Riffel R., Pastoriza M. G., 2010, ApJ, 713, 469

Riffel R., Riffel R. A., Ferrari F., Storchi-Bergmann T., 2011, MNRAS, 416, 493

Riffel R. et al., 2015, MNRAS, 450, 3069

Rodríguez-Ardila A., Mazzalay X., 2006, MNRAS, 367, 57

Rodríguez-Ardila A., Viegas S. M., 2003, MNRAS, 340, 33

Rodríguez-Ardila A., Contini M., Viegas S. M., 2005, MNRAS, 357, 220

Salaris M., Weiss A., Cassarà L. P., Piovan L., Chiosi C., 2014, A&A, 565

Sarzi M., Allard E. L., Knapen J. H., Mazzuca L. M., 2007, MNRAS, 380, 949

Schlesinger K., Pogge R. W., Martini P., Shields J. C., Fields D., 2009, ApJ, 699, 857

Schmitt H. R., Storchi-Bergmann T., Cid Fernandes R., 1999, MNRAS, 303, 173

Springo C. M., Haynes M. P., Giovanelli R., Kent B. R., 2005, ApJS, 160, 149

Storchi-Bergmann T., Wilson A. S., Mulchaey J. S., Binette L., 1996, A&A, 312, 357

Storchi-Bergmann T., Raimann D., Bica E. L. D., Fraquelli H. A., 2000, ApJ, 544, 747

Storchi-Bergmann T., González Delgado R. M., Schmitt H. R., Cid Fernandes R., Heckman T., 2001, ApJ, 559, 147

Storchi-Bergmann T., Riffel R. A. Riffel R., Diniz M. R., Borges Vale T., McGregor P. J., 2012, ApJ, 755, 87

Terlevich R., Melnick J., 1985, MNRAS, 213, 841

Tsvetanov Z., Walsh J. R., 1992, ApJ, 386, 485

Ulvestad J. S., Wilson A. S., 1984, ApJ, 278, 544

Unger S. W., Pedlar A., Axon D. J., Whittle M., Meurs E. J. A., Ward M. J., 1987, MNRAS, 228, 671

Winge C., Riffel R. A., Storchi-Bergmann T., 2009, ApJS, 185, 186

This paper has been typeset from a TEX/LATEX file prepared by the author.